Journal of Structural Geology, Vol. 3, No. 1, pp. 51–65, 1981
Printed in Great Britain

0191-8141/81/010051-14 $02.00/0

An inverse problem in microtectonics for the determination of stress tensors from fault striation analysis

A. ETCHECOPAR

Laboratoire de Géologie Structurale, Université des Sciences et Techniques du Languedoc, 34060 Montpellier-Cédex, France

G. VASSEUR and M. DAIGNIERES

Centre Géologique et Géophysique, LP C.N.R.S., USTL, 34060 Montpellier-Cédex, France

(*Received* 27 *May* 1980; *accepted in revised form* 28 *November* 1980)

Abstract—A method is proposed to compute some characteristics of a possible stress tensor related to striations measured in a given faulted area. If several tectonic phases are responsible for the striations the method separates and determines the successive stress tensors. The iterative algorithm consists of alternatively: (a) sorting the data attributed to a tectonic phase; and (b) computing the characteristics of the stress tensor of this phase. The method is tested using an application to synthetic and actual data.

INTRODUCTION

RECENT studies (e.g. Molnar & Tapponnier 1975) have shown that during orogenesis, brittle deformation is important and affects much larger areas than plastic deformation which is located in the axial zones of orogenic belts. Furthermore, such studies have shown that the analysis of the stress field is the best way to integrate strains of different intensities and natures within the same model. Therefore, in order to control dynamic models, it is of primary importance to determine the local stress state for a given region. In the axial zone of orogenic belts, plastic deformation prevails and depends on too many parameters (pressure, temperature, external rotations, primary anisotropies etc.) to be related simply to the stresses. By contrast, in areas where brittle deformation is prevalent, the deformation is localized along major faults bordering areas where deformation is less important and may be used for the determination of the stress tensors (Mattauer & Mercier 1980). The aim of this contribution is to show that we can determine some elements of one or several successive stress states, using striations measured on fault planes within these slightly deformed areas.

Using the approach of Bott (1959) and Price (1966), several authors (e.g. Carey & Brunier 1974, Carey 1976, Carey 1979, Armijo & Cisternas 1978, Angelier & Goguel 1979, Angelier & Manousis 1980) have proposed quantitative computer-aided methods for the interpretation of various fault plane striations for a given area of faulting. The basic assumptions used are that for a particular place, a given tectonic event is characterized by one homogeneous stress tensor and that for a given phase, the resulting movement (responsible for the striation) has the same direction and sense as the resolved shear stress (physical limits arising from these assumptions will be discussed later).

If the previous assumptions are satisfied, then the deviatoric stress tensor of a tectonic event can be obtained, from several independent data related to this event, to within a multiplicative constant. In the case of superimposed tectonic phases, the problem consists of defining the relevant stress tensors and selecting the corresponding striated fault planes. Methods for picking out the data corresponding to two different tectonic phases have been applied to synthetic and actual data (Armijo & Cisternas 1978, Carey 1979, Etchecopar *et al.* 1980, Angelier & Manousis 1980).

The aim of this work is to present a general method for reducing microtectonic observations in a faulted area. After giving an example of a striated plane, we first develop an inverse technique for computing one stress tensor and apply this technique to a set of data where synchronous movement is insured. We then describe an iterative method applicable to multiphase tectonics where the sorting of the data and the computation of the stress tensors are performed alternatively. When applied to synthetic and actual data, this method is shown to separate successfully several superimposed tectonic phases.

MEASUREMENTS

A typical example of a striated fault plane is shown in Fig. 1. For each plane bearing a striation we define two unit vectors **n** and **s**; **n** is the unit normal which has an upward vertical component, and **s** is the unit vector parallel to the striation and which is orientated parallel to the movement of the upper block with respect to a lower one.

INVERSE PROBLEM APPLIED TO MONOPHASED DATA

Basic assumptions and statement of the problem

Necessary conditions for obtaining quantitative information about the stress tensor using striation data have been given by Arthaud (1969) and Carey (1976). They are summarized as follows. (a) In the considered area the state of stress is homogeneous. In particular the presence of faults does not modify the stress tensor, which can be verified only if the displacements are small compared with fault plane dimensions. (b) The medium is isotropic and the tangential force applied on a given plane results in a tangential displacement in the direction and orientation of this force. (c) No distributed torque exists in the medium, that is the stress tensor is a symmetric one. Using these assumptions, the stress state which is responsible for the observed displacement is characterized, in the referential frame of its principal directions, by a diagonal tensor:

$$\mathbf{T} = \begin{pmatrix} \sigma_1 & 0 & 0 \\ 0 & \sigma_2 & 0 \\ 0 & 0 & \sigma_3 \end{pmatrix} \tag{1}$$

when $\sigma_1 \geqslant \sigma_2 \geqslant \sigma_3$.

This tensor T can be separated into an isotropic pressure part **P** and a deviatoric one **D**. The referential of the principal axes is described by its three Euler's angles (ψ, θ and ϕ, see Fig. 2) with respect to geographical axes *ox*, *y* and *z*(*x*, *y* and *z* are respectively north horizontal, east horizontal, and downward vertical); thus six quantities σ_1, σ_2, σ_3, ψ, θ and ϕ are necessary to define a tensor **T**.

The resulting force on a plane with unit normal **n** has a tangential component $\mathbf{f_t}$ given by (Fig. 3):

$$\mathbf{f_t} = \mathbf{T}\cdot\mathbf{n} - (\mathbf{n}\cdot\mathbf{T}\cdot\mathbf{n})\mathbf{n} \tag{2}$$

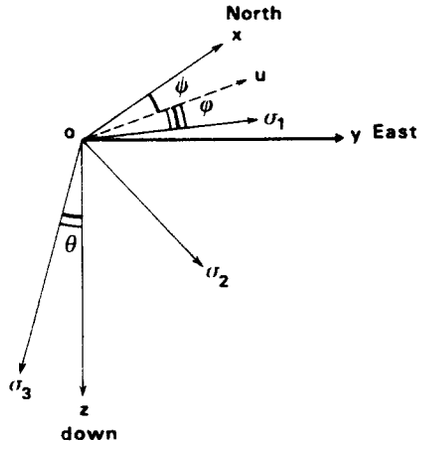

Fig. 2. Euler's angles (ψ, θ and ϕ) describing the three rotations which specify the frame of principal stress directions (σ_1, σ_2, and σ_3) with respect to the geographical reference frame (*ox*, *y* and *z*).

corresponding to a unit vector:

$$\mathbf{t} = \frac{\mathbf{f_t}}{\|\mathbf{f_t}\|}. \tag{2a}$$

Only the deviatoric part **D** of **T** contributes to this tangential force since the pressure part **P** results in a force which is normal to the plane. Moreover the direction and orientation of $\mathbf{f_t}$ (i.e. of **t**) remain unchanged when **T** is multiplied by an arbitrary positive constant. Therefore the unit vector **t** in the direction of the tangential force depends only on four parameters which give (a) the principal directions, i.e. the three Euler's angles ψ, θ and ϕ, and (b) the relative ratio of principal stresses which can be characterized by:

$$R = \frac{\sigma_2 - \sigma_3}{\sigma_1 - \sigma_3} \tag{3}$$

with $0 \leqslant R \leqslant 1$. These four parameters do not define a unique tensor but a set of stress tensors characterized by, for example, one normalized deviatoric tensor $\mathbf{D_0}$ (with $\sigma_1 - \sigma_3 = 1$); every tensor **T** being of the form

$$\mathbf{T} = \lambda\mathbf{D_0} + \mu\mathbf{I} \tag{4}$$

(with $\lambda > 0$ and **I** the unit tensor) belongs to this set and causes, on every plane surface, a displacement with the same unit vector **t**.

As a result of this ambiguity, striated planes can only be expected to give such a normalized deviatoric tensor $\mathbf{D_0}$. In order to obtain the actual tensor, further assumptions must be made for estimates of λ and μ (lithostatic pressure, experimental fracture tests, etc.).

Now consider N fault planes with unit normals $\mathbf{n}_i$ ($i = 1,\ldots N$) on which striations with unit vectors $\mathbf{s}_i$ ($i = 1,\ldots N$) assumed to correspond to the same tectonic stress tensor have been measured. The inverse problem consists of determining the parameters (ψ, θ, ϕ, R) of the tensor $\mathbf{D_0}$ — and via equation (4) of the corresponding set of tensors **T** — which explains the data, i.e. such that for each i, the unit vector $\mathbf{t}_i$ of the tangential force corresponds to the unit vector $\mathbf{s}_i$ of the observed striation (Fig. 3). If we define the vector function $\mathcal{L}_i(\psi, \theta, \phi, R)$ which, for a given $\mathbf{n}_i$, maps (ψ, θ, ϕ, R) into $\mathbf{t}_i$: then

$$\mathbf{t}_i = \mathcal{L}_i(\psi,\theta,\phi,R) = \frac{\mathbf{T}\cdot\mathbf{n}_i - (\mathbf{n}_i\cdot\mathbf{T}\cdot\mathbf{n}_i)\,\mathbf{n}_i}{\|\mathbf{T}\cdot\mathbf{n}_i - (\mathbf{n}_i\cdot\mathbf{T}\cdot\mathbf{n}_i)\,\mathbf{n}_i\|}. \tag{5}$$

The parameters ψ, θ, ϕ and R to be obtained are those which give the 'best agreement' between $\mathbf{t}_i$ and $\mathbf{s}_i$.

Previous methods

At least four striations on independent fault planes are in principal necessary to derive the four parameters ψ, θ, ϕ and R. For $N > 4$ the problem is in general overconstrained and, because of various error causes, it becomes impossible to verify $\mathbf{s}_i = \mathbf{t}_i$ for each fault.

Carey & Brunier (1974) and Carey (1976) define a vector $\mathbf{u}_i$:

$$\mathbf{u}_i = \mathbf{s}_i \times \mathbf{n}_i \tag{6}$$

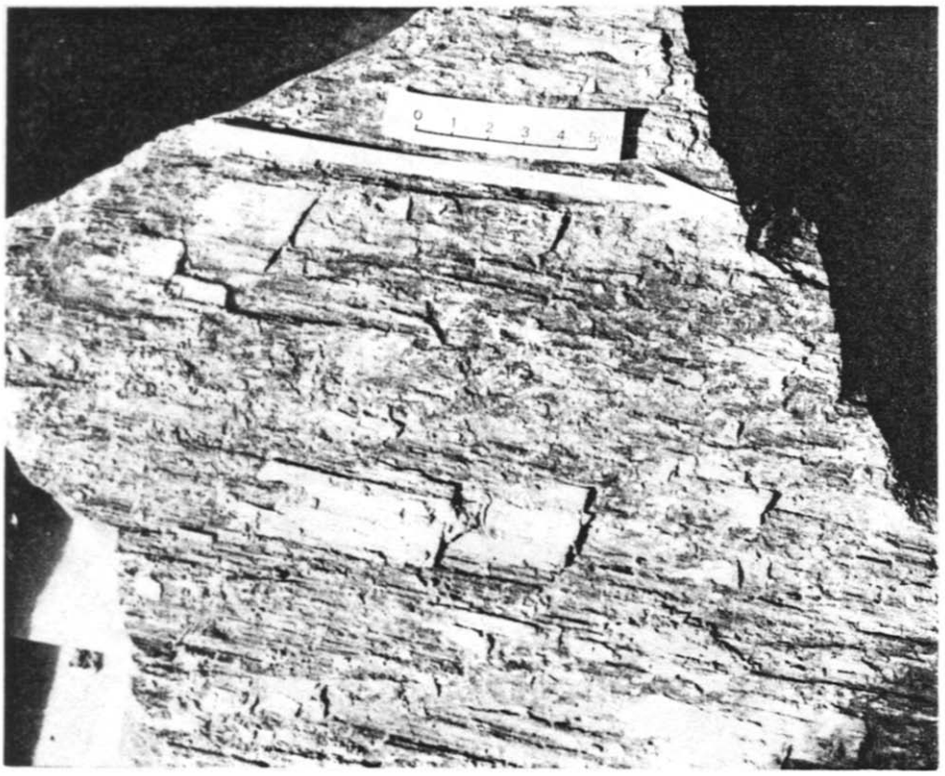

Fig. 1. An example of a striation with an orientation (s) indicated by the arrow.

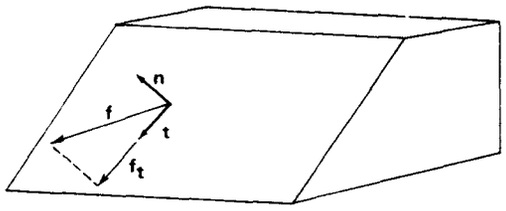

Fig. 3. Block-diagram illustrating a fault plane with normal **n** on which a pressure force **f** is exerted corresponding to a resolved shear stress $\mathbf{f}_t$ with unit vector **t**.

which belongs to the plane and is perpendicular to the observed striation. The parameters of **T** which are calculated by this method are those which give a minimum of

$$\sum_{i=1}^{N} (\mathbf{u}_i \cdot \mathbf{t}_i)^2.$$

Angelier & Goguel (1979) use a least square minimization of the components of calculated tangential stresses perpendicular to the measured striations, that is they search the parameters of **T** which minimize

$$S = \sum_{i=1}^{N} [(\mathbf{n}_i \times \mathbf{s}_i) \cdot (\mathbf{T} \cdot \mathbf{n}_i)]^2. \tag{7}$$

They obtain a mean stress tensor without iteration, but this method cannot be applied if more than one phase is involved in the data.

Armijo & Cisternas (1978) discussed the origin of the angular deviations between the observed striations $\mathbf{s}_i$ and the theoretical ones; these deviations arise from (a) measurements errors on $\mathbf{s}_i$ and $\mathbf{n}_i$, and (b) local fluctuations of the stress tensor. A stochastic approach, using an *a priori* estimate of the covariance matrix of the 'model' (i.e., ψ, θ, ϕ and R) is then used in order to derive the parameters. However this estimate is largely arbitrary; besides, in the proposed method, the three components of $\mathbf{s}_i$ are used as independent data whereas obviously $\mathbf{t}_i$ has only one degree of freedom (since $\mathbf{t}_i \cdot \mathbf{n}_i = 0$ and $\| \mathbf{t}_i \| = 1$) and each striation only corresponds to one scalar datum.

The algorithm developed in this paper is somewhat different from the ones just described; it is also concerned with several improvements concerning the analysis of the angular deviations and also the separation of data corresponding to several different tectonic phases (this last topic is developed in a later paragraph).

Description of the algorithm

The angular deviations between observed and computed striations are assumed to be due to some random noise process arising from measurement and/or from some physical process not accounted for by the model (e.g. local fluctuations of the stress tensor). Therefore, in contrast with the work of Armijo & Cisternas (1978) no further assumption about the model fluctuations needs to be made.

For a given set of N observed striations $\mathbf{s}_i$ ($i = 1, \ldots N$) on fault planes with normal $\mathbf{n}_i$ ($i = 1, \ldots N$), the inverse problem is stated as follows: find the four parameters ψ, θ, ϕ and R of the stress tensor such that the variance of angular deviations defined by:

$$Q = \sum_{i=1}^{N} \langle \mathbf{s}_i, \mathscr{L}_i(\psi, \theta, \phi, R) \rangle^2 \tag{8}$$

is minimum (the bracket $\langle\ \rangle$ denotes the angle between the two vectors). The algorithm is composed of three steps.

Step 1: first estimate. As often occurs in non-linear optimization processes, the choice of an initial parameter set is of primary importance; a wrong choice of initial values may lead to a secondary minimum and therefore to meaningless solutions. The initial choice may be guided by geological arguments, for example using results obtained from data collected at a small distance from the studied area, or using microtectonic structures other than the striated planes (e.g. tension gashes and stylolite peaks allow us to choose σ_3 and σ_1 principal axes respectively of the initial solution); otherwise it is necessary to proceed by trials in the whole range of variations of parameters (ψ, θ, ϕ and R) that is

$$[0, \pi] \times [0, \pi] \times [0, \pi] \times [0, 1].$$

An efficient way of performing such trials consists in using randomly chosen parameters with a uniform probability density over their variation range. Since their variation interval is bounded in $\mathbb{R}^4$, a relatively small number of such trials (50–100) is generally sufficient to obtain an initial solution quite close to the final one, insuring a rapid convergence of the following iterative processes.

Step 2: optimization process. The parameters ψ, θ, ϕ and R obtained in the former step and corresponding to the smallest variance are used as an initial guess for a fast non-linear optimizing procedure using a technique proposed by Rosenbrock (1960) which proceeds by steps in the parameter space, followed by a success or failure test.

Step 3: refinement of the solution, analysis of the angular deviations. The previous step provides a solution (ψ_0, θ_0, ϕ_0, R_0) close to the optimum; it is now possible to linearize around this solution in order to obtain a more refined one. Variance Q, given by (8), is approached by a quadratic form Q' such that:

$$Q \simeq Q' = \sum_{i=1}^{N} (\langle \mathscr{L}_{i0}, \mathbf{s}_i \rangle + \sum_{j=1}^{N} a_{ij} \Delta x_j)^2 \tag{9}$$

($\Delta x_1, \Delta x_2, \Delta x_3, \Delta x_4$) being the increment vector ($\psi - \psi_0$, $\theta - \theta_0$, $\phi - \phi_0$, $R - R_0$) and $a_{i1}, a_{i2}, a_{i3}, a_{i4}$ the partial derivatives of $\langle \mathscr{L}_i, \mathbf{s}_i \rangle$ with respect to ψ, θ, ϕ and R. From classical least square analysis (Linnik 1963) the minimum of Q' is obtained for:

$$\Delta \mathbf{x} = (\mathbf{A}^t \mathbf{A})^{-1} \mathbf{A}^t \mathbf{y} \tag{10}$$

$\mathbf{y}$ being the n-component vector of angular deviations $\langle \mathscr{L}_{i0}, \mathbf{s}_i \rangle$ and $\mathbf{A}$ the matrix (a_{ij}). This process can be iterated until a stable solution is obtained. Note that, when $(\mathbf{A}^t\mathbf{A})$ is ill-conditioned, the classical regularizing technique (Marquardt 1970) is to replace (10) by:

$$\Delta \mathbf{x} = (\mathbf{A}^t \mathbf{A} + \alpha^2 \mathbf{I})^{-1} \mathbf{A}^t \tag{11}$$

(with **I** the unit matrix and α an arbitrary real parameter) which is just identical to the expression used by Armijo & Cisternas (1978).

Using the linearized expression (9), the classical least square theory (Linnik 1963, Hamilton 1964) provides further information about data errors and model uncertainty. To within the linear approximations used, the angular deviations between the observed and theoretical striations have a standard deviation given by:

$$\sigma = \sqrt{\left(\frac{Q_{\min}}{N-4}\right)}, \tag{12}$$

($Q_{\min}$ is the minimum of Q). If $(\psi_0, \theta_0, \phi_0, R_0)$ denotes the optimal model, the actual model belongs, with a confidence level of $(1-\alpha)\,100\,\%$, to that subset of the (ψ, θ, ϕ, R) space defined by

$$Q(\psi,\theta,\phi,R) \leqslant Q_{\min}\left(1 - \frac{4}{N-4}F(N, N-4, 1-\alpha)\right). \tag{13}$$

[$F(\nu_1, \nu_2, p)$ is the F distribution with degrees of freedom ν_1, ν_2]. In the linear approximation which we will assume valid here, the domain defined by (13) is a 4-D hyperellipsoid with $(\psi_0, \theta_0, \phi_0, R_0)$ as a centre; geometrical properties of conjugate directions can then be used in order to derive the max/min of any linear- or linearized-function of ψ, θ, ϕ and R such as, for example, the azimuth and dip of a principal direction.

Another important problem is to find, for each datum, a satisfactory model which is also as close as possible to the optimal one, $\mathbf{T}_0(\psi_0, \theta_0, \phi_0, R_0)$. Define a 'distance' between two tensors $\mathbf{T}_0$ and $\mathbf{T}$ by:

$$d^2(\mathbf{T}, \mathbf{T}_0) = (1 - R_0)^2 \langle \sigma_1^0, \sigma_1 \rangle^2 + R_0^2 \langle \sigma_3^0, \sigma_3 \rangle^2 + \left(\frac{\pi}{4}\right)^2 (R - R_0)^2 \tag{14}$$

$\langle \sigma_i^0, \sigma_i \rangle$ being the angle between the ith principal axis of tensors $\mathbf{T}_0$ and $\mathbf{T}$ (this formula accounts for possible isotropy of the stress tensor).

The problem is to find $\mathbf{T}_i$, a tensor such that: $\langle \mathbf{t}_i, \mathbf{s}_i \rangle = 0$, the 'distance' defined by (14) being a minimum. The solution using a Lagrange multiplier is straightforward. This last analysis may appear to be inconsistent with previous assumptions about the angular deviations; in fact, as will be seen later, it can give information upon the amplitude of possible fluctuations with time and space of the stress tensor.

Case study: synsedimentary tectonics in a Permian basin

As an example of the determination of a stress tensor in the case of a single deformation phase, we have treated a set of 38 striated planes measured in the Saxonian of the Permian Basin of Lodève (Hérault, France). The data list is given in Table 1. The aspect of these striations (which can be described as 'soft' striations) shows clearly that they developed before the sediment was indurated. The Permian sequence comprises of flood-plain sediments deposited in a half-graben limited to the south by a large E–W fault, probably active during sedimentation (Arthaud *et al.* 1977). The stratification dips 20° SE. A horizontal Triassic succession unconformably overlies the Permian (Fig. 4).

Because the material was not completely indurated when the faulting occurred, we expected that the tensor would have been an extensional tensor with the principal axis σ_1 normal to the bedding. However the tensor $\mathbf{T}_1$ obtained from the data (Fig. 5a) has σ_1 axes vertical and a very small R ratio ($R = 0.09$). In order to control this result we have, in a second trial, imposed a tensor $\mathbf{T}_2$ deduced from $\mathbf{T}_1$ by a rotation pulling the principal stress σ_1 in a position normal to the bedding (Fig. 5b). In this case the angular deviations between actual and computed striations are clearly larger than for tensor $\mathbf{T}_1$. Starting from $\mathbf{T}_2$ we have carried out the minimization step and we have obtained a tensor identical to $\mathbf{T}_1$. This result demonstrates that the tilting of the bedding predates the induration of the sediments. It also shows that in a simple case like this one, the tensor axes can be defined with fairly good accuracy.

In Fig. 6(a) the confidence domains at a confidence level of 95 % for each of the principal axes are shown. The one for the σ_1 axes (deviation less than 3·5°) is very small which insures that the tilting was necessarily prior to the tectonic event. The ones for the σ_2 and σ_3 axes are greater and elongated in the horizontal direction; explained by the very low value of the ratio R. For the same confidence level the ratio R has a confidence range between 0.03 and 0.15 which indicates that the direction of the σ_3 axis is significantly determined; in fact the direction of σ_3 is normal to the major normal fault limiting the basin.

For each striated plane we have calculated, as explained in the preceding paragraph, a satisfactory tensor as close as possible to the final solution and displayed as the direction of σ_1 on Fig. 6(b). The deviations with respect to the average computed direction are very small (a few degrees); they may arise from several causes, one of which is discussed in the Appendix (it is shown that, for an elastic medium with an elliptic crack representing a fault, the assumption that the tangential force arising from the regional stress state has to be parallel to the displacements may be erroneous by some degrees).

INVERSE PROBLEM APPLIED TO POLYPHASED DATA

Statement of the problem

In general, rocks in a faulted area have been affected by several successive tectonics events corresponding to several stress tensors. In this case the inverse problem is to obtain the stress tensors and also to sort out from the observed data, the striations which are associated with each tectonic stress tensor. Generally, only a few tectonic phases have affected a given area.

In order to define a tectonic phase (i.e. a stress tensor) and the corresponding striations, the following idea is

Table 1. Field data from the Permian basin of Lodève. Each set of data is composed of a fault plane measurement (St = strike; Pl = Plunge; Q = quadrant) and striation measurement (P = pitch; RD = reference direction for pitch measurement or Az = azimuth when the fault plane is nearly horizontal; SM = sense of movement)

No.	St	Pl	Q	P	RD	Az	SM
1	150	85	E	55	N		N
2	85	58	N	90			N
3	97	75	N	90			N
4	120	70	N	75	W		N
5	125	70	N	80	W		N
6	90	85	N	85	E		N
7	5	75	E	90			N
8	110	65	N	85	W		N
9	100	60	N	90			N
10	100	70	S	90			N
11	85	70	S	90			N
12	120	62	S			09	N
13	100	55	N	90			N
14	129	45	S			35	N
15	122	70	N	75	W		N
16	125	70	N	75	W		N
17	125	46	S			25	N
18	84	75	S	82	W		N
19	120	80	N	70	W		N
20	2	72	E	75	N		N
21	106	74	S	90			N
22	136	65	E	70	N		N
23	10	86	W	85	N		N
24	37	85	W	70	N		N
25	20	70	W	90			N
26	0	85	E	85	S		N
27	85	55	N	75	E		N
28	130	75	N	80	W		N
29	15	86	W	80	N		N
30	30	38	W			114	N
31	95	60	S	75	W		N
32	105	86	N	60	W		N
33	105	75	N	90			N
34	130	75	N	80	W		N
35	110	80	N	70	W		N
36	90	48	N	80	W		N
37	100	49	N	85	E		N
38	20	45	W			95	N

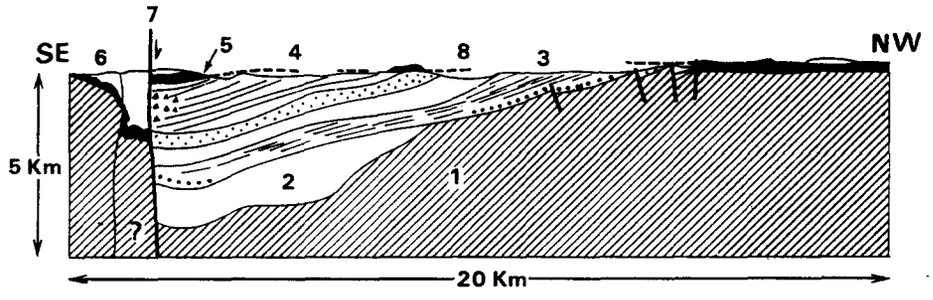

Fig. 4. Cross section of the Permian basin of Lodève (Hérault, France). 1, basement; 2, Stéphanian; 3, Autunian; 4, Saxonian; 5, Trias; 6, post-Triassic series; 7, major normal fault; 8, Triassic unconformity (after Arthaud *et al.* 1977).

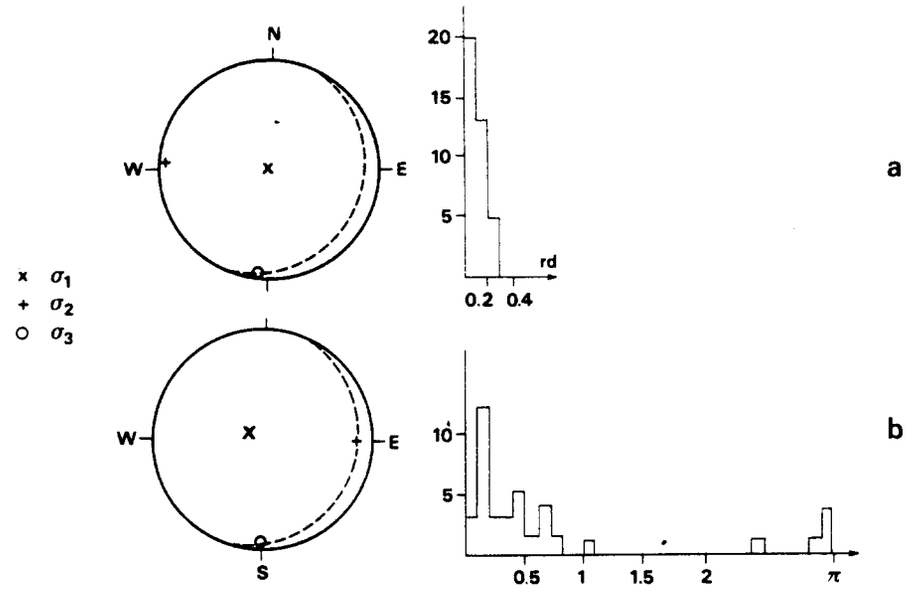

Fig. 5. (a) Schmidt projection (lower hemisphere) of principal stress tensor directions obtained using the method described. The dotted arc corresponds to the bedding. In the histogram of residuals between observed and computed striations the horizontal axis is scaled in radians. (b) Schmidt projection of principal directions of an assumed stress tensor, imposed to be parallel (σ_2 and σ_3) and perpendicular (σ_1) to the bedding. Histogram shows resulting residuals between observed and computed striations.

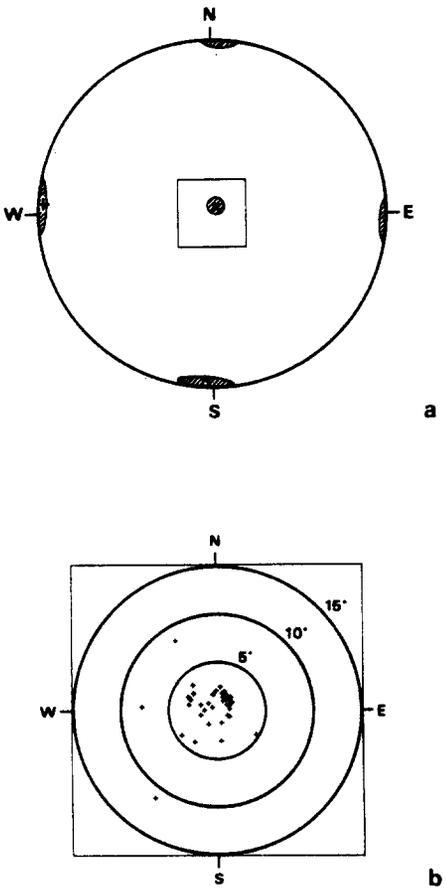

Fig. 6. (a) Schmidt projection of principal stress directions with their confidence domain (at 90% confidence level) displayed by hatched area for σ_1 (×), σ_2 (+) and σ_3 (o) principal stress directions. (b) Enlarged view of the central part of the previous Schmidt projection. Each cross (+) corresponds to the σ_1 direction of a tensor which (i) perfectly explains one datum, and (ii) is as close as possible to the optimal solution given above.

developed; if n data ($n \leqslant N$) are due to the same tectonic phase, the variance of angular deviations is expected to be smaller than if the n data correspond to different phases. Since the number of phases is not known and since no *a priori* information exists about the correspondence between striations and tectonic phases, the algorithm developed below, needs to be tested seriously in order to trust the results obtained.

Description of the algorithm

This is only a modification of the method used in the situation of monophased data.

Step 1: a great number of tensors (100 or more) is tried, using randomly chosen parameters (ψ, θ, ϕ, R); for each of these tensors one calculates for each of the N fault planes the associated theoretical striation direction; the $n < N$ fault planes (for the choice of n see the next paragraph) which give the n smallest angles between the theoretical and actual striations are selected; then the associated quadratic sum S of these n angular deviations is calculated. Among all these tensors, the one with the smallest value of S, $\mathbf{T}_0$, is kept.

Step 2: using as an initial guess the parameters ($\psi_0, \theta_0, \phi_0, R_0$) of $\mathbf{T}$ obtained by step 1 and as an initial selection the n fault planes giving the smallest deviations, modifications of the parameters are performed (as described in the preceding paragraph) in order to minimize the quadratic sum S of the angular deviations for these n selected data. Then a new selection of observed striations is initiated: some data not consistent with the new tensor can eventually be replaced by others not used during the

previous stage and a new optimizing procedure is iterated. This method of alternating optimization and selection was found to converge quickly if, in the initial guess, a broad majority of the data belongs to the same tectonic phase.

Step 3: as for monophased data, it leads to an improved solution with its confidence domain.

The data which are not explained by the computed tensor are used to derive another tensor corresponding to some other phase, the procedure starting from step 1. Eventually, tectonic phases for which confidence domains overlap can be regrouped.

An artificial example with emphasis on the choice of the percentage n/N

A critical point of this method is concerned with the *a priori* choice of the number n of data (or corresponding percentage n/N) on which the minimization has to be carried out. In this section we show on a synthetic example that it is possible to determine an optimum value of n by using several criteria.

In order to provide a synthetic example, three sets of data from several regions have been mixed together; each set corresponds to a particular tensor already well determined. Twenty-four data out of 48 (i.e. 50%) correspond to a first tensor T_1; and 11 and 13 data respectively correspond to the second and the third tensors, T_2 and T_3. The three tensors T_1, T_2 and T_3 are shown on Fig. 7(a).

When using all data, as for the monophased example, the obtained tensor (Fig. 7b) is the same for every random choice of the initial solution; it is a compromise between the three actual tensors shown on Fig. 7(a), and the histogram of associated angular deviations is flat (Fig. 7c). Moreover, for all the angular deviations (even the smallest), data belonging to each of the three tensors T_1, T_2 and T_3 are mixed together. Therefore if selection of data is not performed the solution obtained is without significance.

For each of the following percentages: 30, 40, 50, 60 and 70%, three trials have been carried out from different initial solutions. In Fig. 8 we give for each trial the histogram of angular deviations between actual and computed striations, the ratio R and the projection on a Schmidt net (lower hemisphere) of the principal σ_1 and σ_3 axes.

For a percentage of 30 or 40% (values lower than the actual percentage for the first tensor), the angular deviations between actual striations and computed ones are small; however for the three different initial solutions (obtained from random choice), the optimization process leads to tensors which are quite remote one from each other (especially in the 30% case) and the striated planes taken into account are different for each solution. Thus the final solution is not stable with respect to the initial one; in other words different initial choices result in different final solutions. Moreover in some cases, it is clear that some striations are not taken into account despite the fact that the angle between the observed striation and the computed one remains reasonably small.

For percentage values of 60 and 70% (values greater

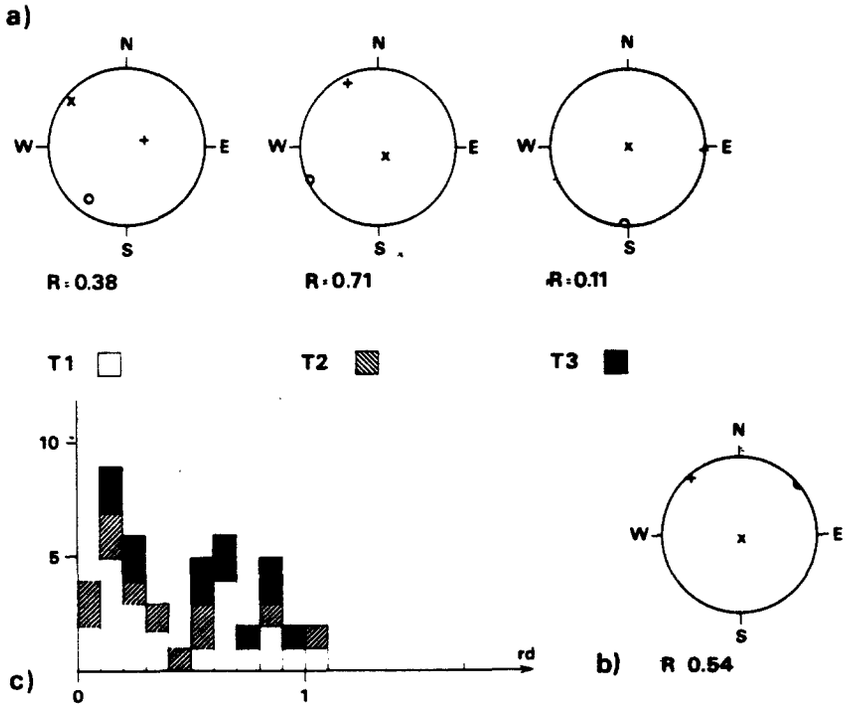

Fig. 7. (a) Schmitt projection of principal directions of the three actual stress tensors (T_1, T_2, T_3) with their R ratio (symbols ×, +, o as in Fig. 5. (b) Optimal tensor (principal direction and R ratio) computed using the whole set of data. (c) Histogram of residuals. To each residual, is associated a colour code (white, hatched and black) which specifies which set (T_1, T_2, T_3) the corresponding data originates from.

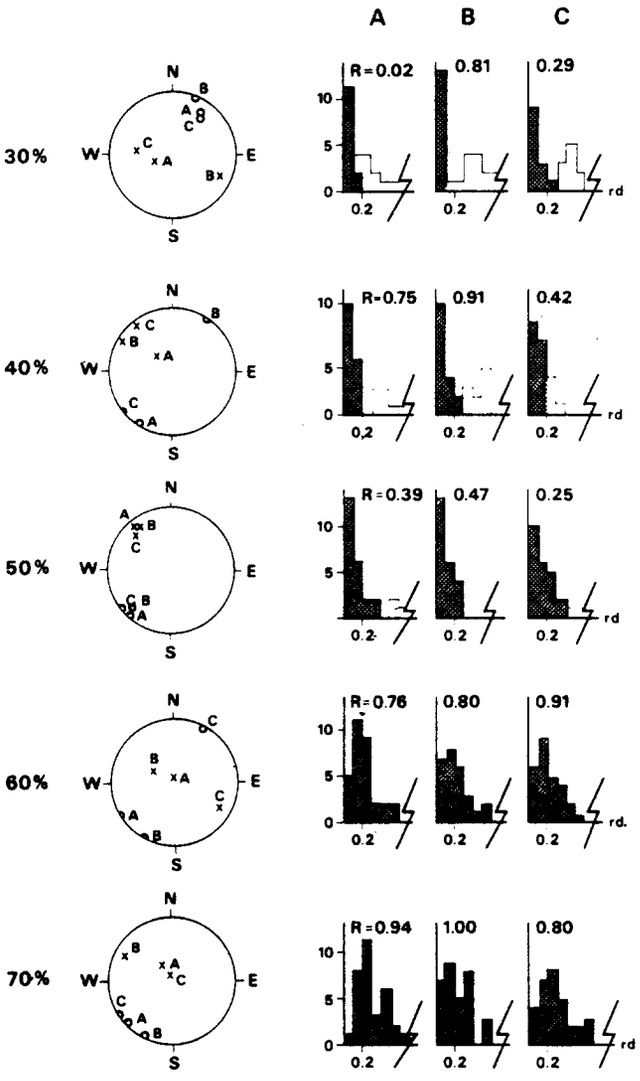

Fig. 8. For 5 different percentages of retained data (30, 40 to 70%) — from top to bottom — three trials of the method labelled A, B and C are performed. On the left part, the principal directions σ_1 (×), σ_3 (o) of computed tensors are displayed and, on the right part, the histograms of residuals for each trial are given together with the computed R ratio. The hatched area corresponds to those data of the set which are accounted for.

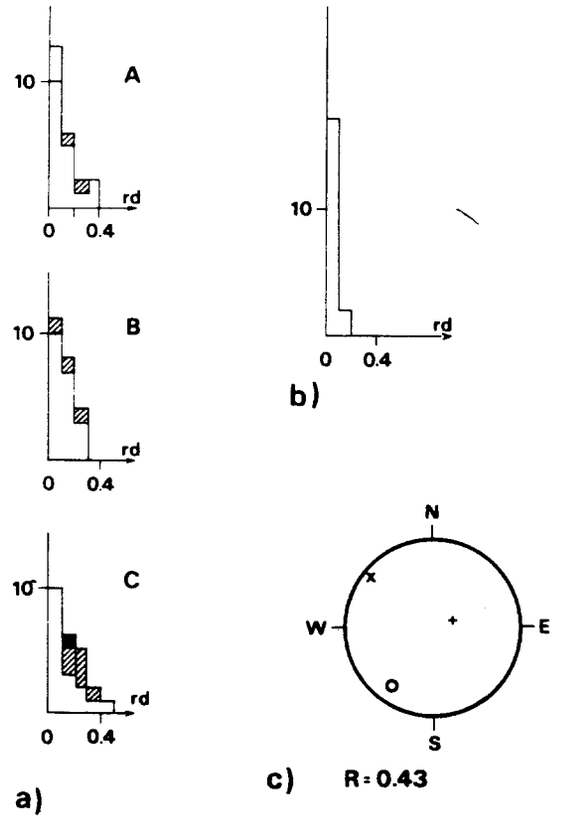

Fig. 9. (a) Details of the three histograms obtained in trials A, B and C with a percentage value of 50% (cf. Fig. 8). Only the data accounted for in the computation are shown with a code which specifies from which set (T_1, T_2, T_3, cf. Fig. 7) they originate. (b) Histogram of residuals obtained when using the 19 data which are common to trials A, B and C. (c) Resulting tensor obtained from these 19 data characterized by its principal stress directions and R ratio (compare with the actual T_1 tensor of Fig. 7a).

than the actual largest one) the final solution is again observed to be unstable with respect to the initial one. The histogram of the angular deviations becomes flat with the maximum displaced toward greater deviations.

In contrast with the previous results, for a value of 50% (i.e. the actual value), the final solutions appear to be very stable for various initial solutions: the resulting tensors are very close to each other. Out of the 24 data chosen, 19 remain the same for the three starting solutions (Fig. 9a); and it is verified that these 19 data are actually issued from the first set of data corresponding to tensor T_1. If minimization is performed using only these 19 data, the resulting tensor is very close to the tensor T_1 (Figs. 9b and c). For each of the 48 striated planes we have calculated the angular deviation between actual and computed striations; it appears then that data issued from the two other sets exhibit very small deviations.

Therefore the percentage of measures which will be chosen for the minimization is the one which: (a) leads to stable solutions after the minimizations calculated for different random trials; (b) takes into account a maximum number of striations giving small deviation (a threshold of 20° is generally adequate); and (c) gives histograms for which the maximum corresponds to the smallest differences in angle.

AN EXAMPLE OF PHASE SEPARATION WITH APPLICATION TO LANGUEDOC TECTONICS

The example selected for analysis is a 150 m long calcareous outcrop situated at Prades, north of Montpellier (Hérault, France). The structural setting is given in Fig. 10. A detailed cross-section of the studied area is given in Fig. 11. The example was chosen because it shows brittle microstructures characteristic of the Languedoc (Arthaud & Mattauer 1969, Arthaud in press). The measurement of striations was carried out on decimetric- to metric-scale fault planes which cut relatively massive Berriasian limestones. Sixty-four striated planes have been selected in a manner to present a

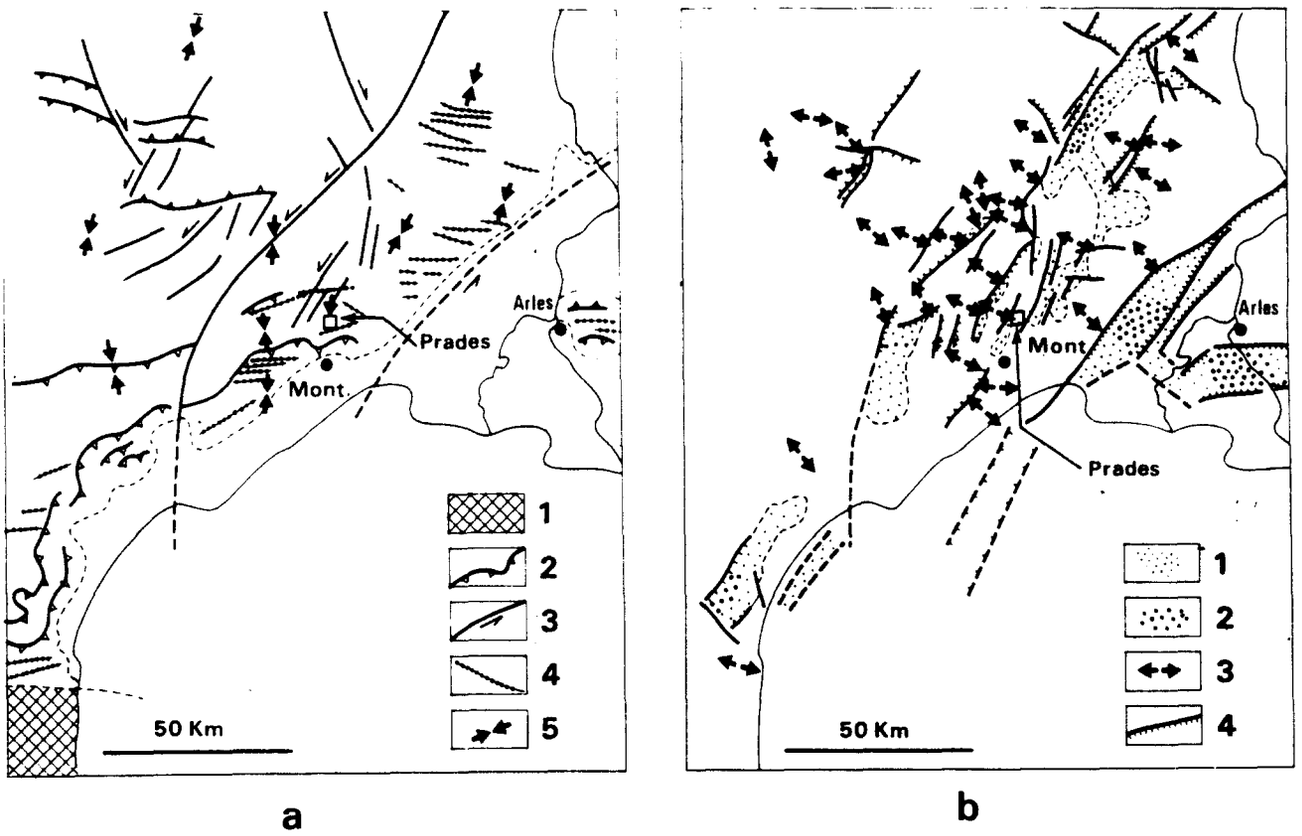

Fig. 10. (a) Structural setting of the studied area during the Pyrenean phase. 1, Pyrenean axial zone; 2, main overthrust; 3, transverse fault; 4, fold axis; 5, compression direction. (b) Structural setting at the studied area during the Oligocene. 1, Oligocene basin with thickness under 1000 m; 2, Oligocene basin with thickness in excess of 1000 m; 3, extension direction; 4, main normal fault (after Arthaud *et al.* 1977). The studied outcrop is located at Prades.

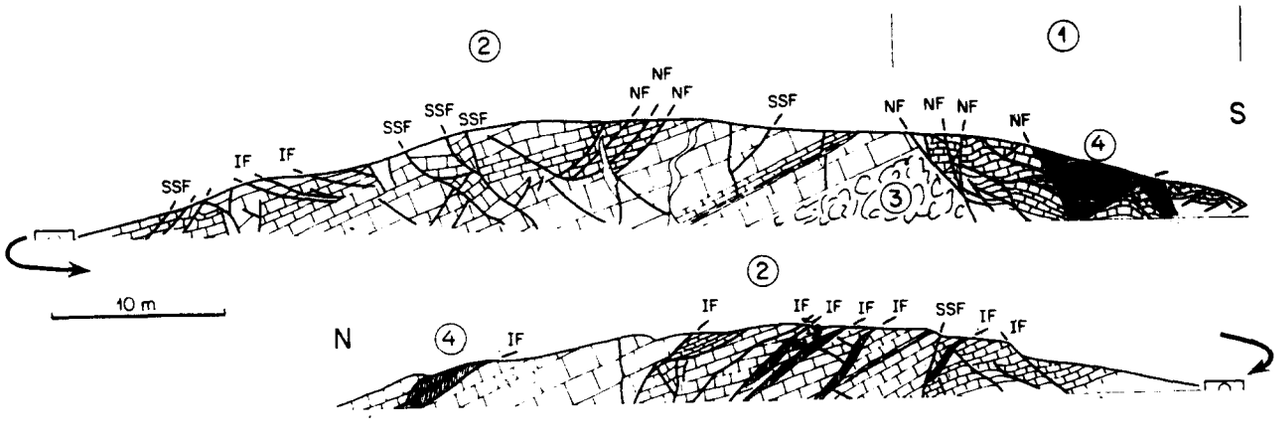

Fig. 11. Schematic cross-section of the outcrop at Prades (north of Montpellier. 1, main normal fault zone (Valanginian); 2, zone of measurement (Berriasian); 3, Berriasian slumps; 4, dissolution cleavage; IF, reverse fault; NF, normal fault; SSF, strike-slip fault.

maximum spatial dispersion. The dip of the stratification varies along the outcrop from 25 to 40° towards the NW. This tilting is attributed by Arthaud (in press) to an Oligocene extensional phase, the last important tectonic phase in Languedoc. The position before the tilting has therefore been recalculated for each striated fault plane. The data list is given in Table 2.

Treatment of the measurements

The treatment of the measurements by the method previously described leads to four tensors which are presented in the Table 3 in a chronological order suggested by comparison with other work in the Languedoc area which is discussed later.

Table 2. Field and rotated data from the calcareous outcrop of Prades, north of Montpellier. For each data set are given the bedding characteristics, the actual field measurements, and the data characteristics obtained through a rotation which returns the bedding to horizontal

No.	Bedding			Fault field measurements							Rotated fault measurements				
	St	Pl	Q	St	Pl	Q	P	RD	Az	SM	St	Pl	Q	Az	SM
1	38	29	W	44	32	N	24	E		S	86.04	4.27	N	19.23	R
2	38	29	W	58	39	N	36	E		S	94.87	14.89	N	19.16	R
3	38	29	W	70	31	N			28	S	135.01	15.96	E	18.60	R
4	38	29	W	58	56	N	18	E		S	72.25	29.91	N	39.10	R
5	38	29	W	52	42	N			42	S	75.95	15.26	N	37.15	R
5 bis	38	29	W	52	42	N			14	S	75.95	15.26	N	3.64	S
5 ter	38	29	W	52	42	N			156	N	75.95	15.26	N	149.43	N
6	38	29	W	146	40	W			11	N	110.08	39.98	S	31.00	N
7	38	29	W	48	53	N	10	E		S	57.29	24.82	N	37.55	S
8	38	29	W	156	74	W	37	N		D	145.10	62.62	W	141.32	D
9	38	29	W	124	86	W	28	N		D	122.56	88.44	S	122.59	D
10	38	29	W	120	40	S			172	N	92.76	51.20	S	14.05	N
11	38	29	W	46	37	S			140	N	43.27	65.82	E	150.95	N
12	38	29	W	80	31	N			62	S	141.20	20.73	E	54.22	R
13	38	29	W	72	54	N	36	E		S	94.31	32.94	N	32.36	R
14	38	29	W	120	47	S			152	N	97.91	56.83	S	165.85	N
15	38	29	W	88	49	N	33	E		R	117.59	36.00	N	49.25	R
16	38	29	W	74	35	N			48	S	126.52	19.71	N	38.18	R
17	38	29	W	16	25	W			58	R	96.59	10.69	S	63.61	R
18	42	20	W	153	40	W			50	R	127.66	37.00	S	64.51	R
18 bis	42	20	W	132	44	S	57	S		N	112.50	47.47	S	14.61	N
19	42	20	W	178	36	W			70	R	148.46	25.20	W	79.50	R
20	42	20	W	11	31	W			42	R	156.64	16.97	W	48.04	R
21	71	29	N	176	67	W	73	S		N	162.22	62.79	W	102.19	N
22	71	29	N	10	53	W	90			N	164.84	44.43	W	121.67	N
23	71	29	N	130	3	W			134	S	76.06	30.64	S	130.72	N
24	71	29	N	168	28	W			2	R	121.95	36.87	S	6.42	R
25	71	29	N	36	38	W	36	S		R	170.49	20.98	W	77.24	R
26	71	29	N	138	86	W	33	N		D	138.80	82.65	E	139.60	D
27	71	29	N	176	35	W	30	S		R	135.24	37.96	W	32.11	R
28	60	30	N	62	22	W			8	R	54.64	8.05	S	6.05	N
29	60	30	N	145	37	W	59	W		R	13.43	48.29	S	101.83	S
30	60	30	N	148	57	W	54	S		R	130.45	62.80	S	36.47	R
31	60	30	N	162	58	W	48	N		D	142.29	56.83	W	135.52	D
32	60	45	N	68	25	N			26	R	50.32	20.48	S	23.38	D
33	60	45	N	154	60	W	55	S		R	130.21	66.65	S	74.65	R
34	60	45	N	74	34	N			40	R	26.26	14.10	E	31.58	S
35	60	45	N	126	64	S	74	E		R	115.30	87.05	S	108.80	S
36	60	45	N	58	66	W	42	E		R	54.91	21.06	N	18.75	S
37	60	45	N	60	50	N	65	E		R	60.00	5.00	N	175.08	R
38	60	45	N	64	50	N	65	W		R	91.90	5.80	N	127.57	R
39	60	45	N	36	60	W	44	N		R	00.30	24.08	W	1.06	S
40	60	45	N	0	80	W	56	S		R	164.80	61.90	W	95.26	R
41	60	45	N	120	57	S	90			R	106.82	84.92	S	100.33	S
41 bis	60	45	N	120	57	S	18	E		R	106.82	84.92	S	114.28	D
42	60	45	N	20	34	W	10	S		D	111.75	27.24	S	40.44	R
43	60	45	N	53	45	W	25	N		S	147.52	4.94	W	29.96	N
44	60	45	N	121	90		26	W		D	128.60	69.95	N	123.29	D
45	60	45	N	58	57	N	81	W		R	51.97	12.10	N	139.68	R
46	60	45	N	172	70	W	27	N		D	150.46	60.61	W	161.57	D
47	60	45	N	50	90		25	E		S	46.00	45.86	N	35.32	S
48	60	45	N	70	85	N	25	E		S	75.31	40.94	N	46.73	S
49	64	28	N	144	20	W			170	R	98.31	36.70	S	173.61	R
50	64	28	N	156	36	W	45	W		R	122.38	43.62	S	120.82	S
51	64	28	N	150	21	W			175	R	101.83	35.65	S	179.59	R
52	64	28	N	42	74	N	25	W		S	35.29	48.56	W	63.11	S
53	64	28	N	64	34	N			12	R	64.00	6.00	W	7.20	R
54	64	28	N	68	68	N	6	E		S	69.76	40.09	N	62.92	S
55	64	28	N	157	40	W	65	W		R	126.80	46.20	S	109.30	S
56	70	29	N	62	25	W	16	W		R	108.72	5.40	S	78.97	S
57	58	24	N	176	80	E	25	N		D	177.55	88.31	W	177.44	D
58	77	36	N	42	33	E	70	E		N	56.91	65.40	S	81.90	D
59	77	36	N	72	35	N	43	E		R	145.97	3.07	W	29.90	N
60	77	36	N	140	78	W	17	N		S	138.08	84.67	E	136.68	S

Table 3. Characteristics of the 4 tensors obtained at the outcrop of Prades (north of Montpellier). (s etc.) indicates the confidence domain at a confidence level of 95%

phase number	σ_1		σ_2		σ_3		R	s.d. of residuals	n number of data
	Az.	Dip.	Az.	Dip.	Az.	Dip.			
1	(*)	(*)	(*)	(*)	307° (5)	7° (5)	0.92 (0.09)	7.6	12
2	204° (19)	4° (6)	294° (17)	5° (8)	(**)	84° (13)	0.18 (0.09)	6.7	26
3	288° (13)	1° (15)	198° (12)	3° (16)	(**)	87° (15)	0.72 (0.13)	5.2	12
4	(**)	83° (13)	15° (9)	7° (10)	285° (1)	3° (12)	0.40 (0.11)	6.9	13

* Indicates nearly asymmetrical tensors ($R \simeq 0$ or $R \simeq 1$). In these cases only the characteristics of the revolution axis are significant.
** Indicates a nearly vertical direction; in this case the corresponding azimuth has no significance.

From the sixty-four studied faults, only one does not correspond to any of the calculated tensors. In the field, this fault forms in association with another striated fault plane a dihedron, and probably represents a parasitic movement imposed by the geometry. Therefore it cannot be accounted for using our previous assumptions. Figure 12 summarizes the results.

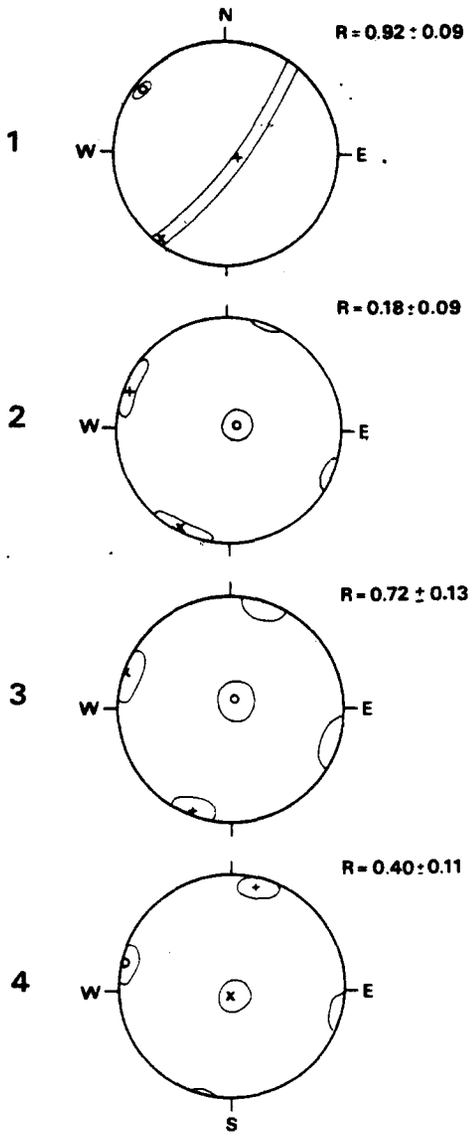

Fig. 12. Display of the principal directions (and confidence domain) and R ratios of the four tensors labelled 1–4 deduced from the data (cf. Table 3).

Comparison with other microstructures

In order to control our results, the distribution of stylolites and tension gashes has been studied. Stylolites are surfaces of preferential dissolution presenting irregularities or stylolitic peaks. Previous studies have shown that the peaks have an average direction parallel to the principal stress direction, σ_1, responsible for their formation. Arthaud (1969) described in the studied outcrop 96 stylolitic peaks that he attributed to the major Pyrenean phase (Fig. 13a). His diagram is comparable with the diagram given here for the direction of the principal stress, σ_1, of the second tensor (Fig. 12): the computed major stress axes σ_1 corresponds exactly to the maximum density of stylolitic peaks. Furthermore, the dispersion of the peak directions coincides with the fluctuations of the tensor about this average position (as

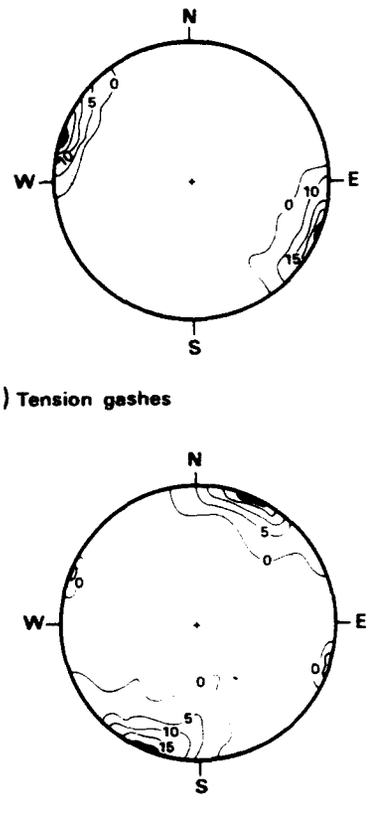

Fig. 13. (a) Density diagram (Schmidt projection, lower hemisphere) of stylolitic peak directions. Vertical peaks are not displayed. (b) Density diagram of directions normal to tension gashes.

explained in the section on monophased data). There are also stylolites with horizontal NE 110° peaks in agreement with tensor number 3. Finally, there are numerous stylolitic peaks perpendicular to the stratification corresponding to tensor number 4 (these peaks are not shown on Fig. 13a).

It is well known that tension gashes appear on the average along planes perpendicular to the σ_3 direction. Thus we have made a systematic analysis of these microstructures. However, in the field, the true tension gashes are difficult to separate from calcite infillings along faults or joints between blocks. On the other hand the anisotropy due to stratification influences the position in space of the gashes. In the case described here we would expect to find a large number of horizontal gashes corresponding to tensors numbers 2 and 3 for which the minimum stresses, σ_3, are vertical. In fact such gashes are rare in the outcrop because they would be parallel to the beds which are less than 1 m thick. However, in a neighbouring quarry where the beds are thick, tension gashes parallel to the stratification are more numerous. Figure 13(b) shows that the maximum of the tension gash planes has an orientation N 30° E which may correspond to tensors numbers 1 or 4; there is no possibility of distinguishing between them.

Relations with Languedoc tectonics

Since Cretaceous time two important tectonic phases have affected the rocks in Languedoc: first a so-called Pyrenean compressive phase, N–S to N 40° E of Eocene age; and secondly an Oligocene phase of extension in a N 120° E direction.

The Pyrenean phase (Fig. 10a) was responsible for the main tectonic structures of Languedoc. It produced thrusts, folds and important strike-slip faults all of which allow the average direction of compression to be determined as N 00–N 30° E. Perturbations exist locally, particularly in the neighbourhood of large faults. Tensors number 1 and 2 are attributed to this phase, both corresponding to a compression directed N 25°E. Tensor number 1 whose intermediate stress σ_2 is vertical may be responsible for a bounding strike-slip fault and occurred before tensor number 2 whose minimum stress, σ_3, is vertical. This chronology is justified by the fact that conjugate strike-slip faults are tilted by a later folding throughout Languedoc.

Locally, there are microstructures indicating a former E–W compression which we attribute to tensor number 3. The chronology of this phase with respect to the others is difficult to determine precisely. Arthaud (in press) proposed that this compression could correspond to an early Pyrenean phase. However, it is difficult to separate in time this episode from the N 20° E compression. An alternative explanation is that the microstructures corresponding to this E–W compression resulted from a local secondary effect (stress deviation) of the N 20° E Pyrenean compression for boundary conditions which still remain to be determined. Rispoli (in press) shows that such perturbations exist around metric- to decametric-scale strike-slip faults.

We attribute tensor number 4 to the Oligocene extensional phase which affected all of Languedoc and created numerous normal faults trending N 20–N 40° E of which the most important limit large basins of continental sediments (Fig. 10b).

Conclusion

The four tensors determined correspond to the observed microstructures and reciprocally there are no inexplicable microstructures at the scale of the outcrop. Moreover, three of the four tensors correspond to the three well known tectonic phases of Languedoc.

CONCLUSIONS

Using a few assumptions, it is possible to give a quantitative interpretation in terms of stresses from striations observed on fault planes. A crucial problem for this interpretation consists in the separation of tectonic phases and of related observations; an algorithm for solving the problem has been proposed. Applied on synthetic data as well as on actual field data, the algorithm was shown to yield fairly satisfactory results. Besides, confidence domains for the parameters of the stress tensor can be determined for each phase.

The proposed method does not require information other than the observed striations: an initial solution is automatically provided using a random exploration of the bounded parameter set. However, it is also possible to take into account various geological constraints such as information deduced from stylolites, tension gashes or observations arising from general studies. In this situation one or several principal directions of the stress tensor may be inferred.

The method has already proved its value for studying various geological problems (Burg & Etchecopar 1979, Santouil 1980). In a platform area which has undergone only slight deformation, it is possible to determine several tectonic phases using indirect observations. Use of the method in slightly deformed areas external to orogenic belts would make it possible to control their geodynamical interpretation.

Acknowledgements—We wish to thank three anonymous referees for their comments which substantially improved the presentation of our argument.

REFERENCES

Angelier, J. & Goguel, J. 1979. Sur une méthode simple de détermination des axes principaux des contraintes pour une population de failles. *C. r. hebd. Séanc. Acad. Sci., Paris* **288**, 307–310.

Angelier, J. & Manousis, S. 1980. Classification automatique et distinction des phases superposées en tectonique de faille. *C. r. hebd. Séanc. Acad. Sci., Paris* **290**, 651–654.

Armijo, R. & Cisternas, A. 1978. Un problème inverse en microtectonique cassante. *C. r. hebd. Séanc. Acad. Sci., Paris* **287**, 595–598.

Arthaud, F. 1969. Détermination graphique des directions de raccourcissement, d'allongement et intermédiaire d'une population de failles. *Bull. Soc. géol. Fr.*, 7 *Ser.* **11**, 729–737.

Arthaud, F. & Mattauer, M. 1969. Sur les décrochements NE–SW senestre contemporains des plis pyrénéens du Languedoc. *C. r. som. Soc. géol. Fr.* **8**, 290.

Arthaud, F., Megard, F. & Seguret, M. 1977. Cadre tectonique de quelques bassins sédimentaires. *Bull. Centres Rech. Explor.–Produc. Elf Aquitaine* **1**, 147–188.

Arthaud, F. in press. Microtectonique et champ de contraintes: exemple de la déformation d'âge paléocène dans l'avant pays alpin en France. *Bull. Soc. géol. Fr.*

Bott, M. H. P. 1959. The mechanics of oblique slip faulting. *Geol. Mag.* **96**, 109–117.

Burg, J. P. & Etchecopar, A. 1980. Détermination des systèmes de contraintes liés à la tectonique cassante au coeur du Massif Central français: la région de Brioude (Haut-Allier). *C. r. hebd. Séanc. Acad. Sci., Paris* **290**, 397–400.

Carey, E. & Brunier, B. 1974. Analyse théorique et numérique d'un modèle mécanique élémentaire appliqué à l'étude d'une population de failles. *C. r. hebd. Séanc. Acad. Sci., Paris* **279**, 891–894.

Carey, E. 1976. Analyse numérique d'un modèle mécanique élémentaire appliqué à l'étude d'une population de failles: calcul d'un tenseur moyen des contraintes à partir de stries de glissement. Thèse 3ème cycle. Centre d'Orsay.

Carey, E. 1979. Recherche de directions principales de contraintes associées au jeu d'une population de failles. *Rev. Geol. Dyn. Geophys.* **21**, 57–66.

Chinnery, M. A. 1966. Secondary faulting, 1, theoretical aspects. *Can. J. Earth Sci.* **3**, 163–174.

Etchecopar, A., Vasseur, G. & Daignieres, M. 1980. Méthode informatique de séparation de phases en microtectonique cassante. In *8th Réunion Annuelle des Sciences de la Terre, Marseille* 1980. (edited by *Soc. géol. Fr.*) Paris, 141.

Hamilton, W. C. 1964. *Statistics in Physical Science. Estimation, Hypothesis Testing and Least Squares.* Ronald Press, New York.

Kassir, M. K. & Sih, G. C. 1967. Griffith's theory of brittle fracture in three dimensions. *Int. J. Eng. Sci.* **5**, 899–918.

Linnik, Y. V. 1963. *Méthode des Moindres Carrés. Eléments de la Théorie du Traitement Statistique des Observations.* Dunod, Paris.

Marquardt, D. W. 1970. Generalized inverses, ridge regression biased linear estimation and non-linear estimation. *Technometrics* **12**, 591–612.

Mattauer, M. & Mercier, J. L. 1980. Microtectonique et grande tectonique. *Mém. h. sér. Soc. géol. Fr.* **10**, 141–161.

Molnar, P. & Tapponnier, M. 1975. Cenozoic tectonics of Asia: effects of a continental collision. *Science, N.Y.* **189**, 419–426.

Price, N. J. 1966. *Fault and Joint Development in Brittle and Semi-Brittle Rock.* Pergamon Press, Oxford.

Rispoli, R. in press. Brittle kink bands and stress variations in limestones of Languedoc (Southern France). *Tectonophysics.*

Rosenbrock, H. H. 1960. An automatic method for finding the greatest or least value of a function. *Comput. J.* **3**, 175–184.

Santouil, G. 1980. Etude microtectonique comparée des bassins permiens du Sud du Massif Central français Rodez, St Afrique et Lodève. Thèse 3e cycle, Montpellier.

APPENDIX

There are at least four explanations for the presence of angular deviations between observed and computed striations:

(a) the data are not perfect (it is difficult to measure with an error of only a few degrees the orientations of 'fault planes' and striations);

(b) local fluctuations of the stress tensor can be associated with faults (Chinnery 1966);

(c) when two or more tectonic phases have followed each other, small strains caused by one phase can change in a heterogeneous way the orientations of structures related to older phases; and

(d) when the fracture surface is of an elongated shape it is possible that the tangential force applied on the plane and the resulting striations are not exactly parallel to each other. Kassir & Sih (1967) have obtained an approximate solution for the strain around an elliptical surface of discontinuity in an elastic medium subjected to a uniform stress field: if the crack is an ellipse (Fig. 14) with centre 0, major and minor semiaxes a and b, parallel to Ox and Oy, the angles $\psi = (Ox, s)$ and $\omega = (Ox, t)$, where s and t are calculated at 0, are binded by: $H \cdot \tan\psi = \tan\omega$, where

$$H = \frac{(k^2 + \nu k'^2)E(k) - \nu k'^2 K(k)}{(k^2 - \nu)E(k) + \nu k'^2 K(k)}$$

with

$$k^2 = \frac{a^2 - b^2}{a^2}, \qquad k' = \frac{b}{a},$$

ν being Poisson's ratio of the medium, $K(\ )$ and $E(\ )$ being respectively the complete elliptical integral of the first and second kind. Table 4 shows the discrepancy between s and t for four values of the ratio $k' = a/b$ of the fracture; it can be bigger than 8° for a fault with an elongation coefficient of ten. As fault planes are commonly elongated this can play an important part in the observed residuals.

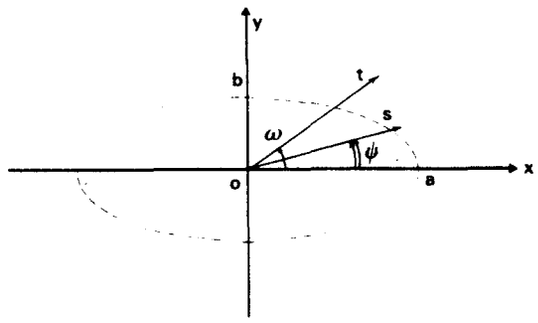

Fig. 14. Model of an elliptical crack in the oxy plane with major and minor axes along ox and oy, s is unit vector of the displacement at point o and t the unit vector of the tangential force (resolved shear stress) corresponding to the regional stress, that is far from the crack.

Table 4. Value of the angular difference $\omega - \psi$, between the striation and resolved shear stress on fault plane as a function of ω and k' (see text)

ω \ k'	1	2	5	10
0°	0°	0°	0°	0°
20°	0°	1.1°	3.9°	4.9°
45°	0°	1.7°	6.6°	8.5°
70°	0°	1.1°	4.6°	6.2°
90°	0°	0°	0°	0°